MICROBIAL GENOMICS

RESEARCH ARTICLE

Park *et al.*, *Microbial Genomics* 2020;6

DOI 10.1099/mgen.0.000464

Comparative genomics of wild-type and laboratory-evolved biofilm-overproducing *Deinococcus metallilatus* strains

Chulwoo Park[1], Bora Shin[1], Wonjae Kim[1], Hoon Cheong[1], Soyoon Park[2] and Woojun Park[1,*]

Abstract

Deinococcus metallilatus MA1002 was exposed to ultraviolet radiation to generate mutants with enhanced biofilm production. Two strains (nos 5 and 6) were then selected based on their high biofilm formation, as well as their possession of higher concentrations of extracellular matrix components (eDNA, protein and saccharides) than the wild-type (WT). Genomic sequencing revealed the presence of large genome deletions in a secondary chromosome in the mutants. Expression analyses of the WT and mutant strains indicated the upregulation of genes associated with exopolysaccharide synthesis and stress response. The mutant strains showed high mortality in glucose-supplemented (TYG) medium; however, cell death and biofilm formation were not increased in mutant cells grown under acetate- or glyoxylate-added media, suggesting that metabolic toxicity during glucose metabolism induced a high rate of cell death but improved biofilm formation in mutant strains. In damaged cells, eDNAs contributed to the enhanced biofilm formation of *D. metallilatus*.

DATA SUMMARY

All genome data files have been deposited in the National Center for Biotechnology Information (NCBI) GenBank database under the following accession numbers: *Deinococcus metallilatus* MA1002 WT, CP038510--CP038512; no. 5 mutant, VBRC00000000; and no. 6 mutant, SDEC00000000. Additionally, RNA-seq data were deposited in the NCBI Gene Expression Omnibus database (GSE130360).

INTRODUCTION

Deinococcus spp. are robust bacteria that carry an extraordinary DNA repair system that allows them to survive under multiple stress conditions, including oxidative stress, ionizing and ultraviolet (UV) irradiation, and desiccation [1–3]. *Deinococcus radiodurans*, a model *Deinococcus* species, is capable of withstanding 5000 Gy of γ-irradiation and 624 J m^{-2} of radiant exposure, which are approximately 310- and 20-fold higher than the doses commonly used to kill *Escherichia coli*, respectively [2, 4, 5]. Similar to other bacteria, *Deinococcus* spp. also exhibit a RecA-dependent DNA repair mechanism (i.e. a major DNA double-strand-break repair system) several hours after irradiation; however, a RecA-independent mechanism is activated in *D. radiodurans* during the first 1.5 h after irradiation [3].

Biofilm formation occurs as micro-organisms irreversibly adhere to and grow on a surface, where they secrete extracellular polymers [6]. This process alters the micro-organism's phenotypes, including growth rate and gene transcription [6]. Bacteria naturally form biofilms as a protective mechanism against stress [7]. Biofilms are composed of bacterial consortia and secreted substances referred to as the extracellular matrix (ECM), which mainly consist of several exopolysaccharides (EPSs), eDNAs and proteins [7]. These components interact firmly with each other, creating robust biofilms to increase survivability under unfavourable environmental conditions [8]. Many studies have demonstrated that crosslinked EPSs can store water and act as a hydration buffer, thereby providing high tolerance to desiccation [9]. EPSs could also help protect cells from UV radiation by absorbing photons and are also known to scavenge reactive oxygen species [9].

Given that *Deinococcus* spp. are highly resistant to a variety of stressors, their ability to form biofilms under harsh conditions,

Received 28 July 2020; Accepted 15 October 2020; Published 04 November 2020

Author affiliations: [1]Laboratory of Molecular Environmental Microbiology, Department of Environmental Science and Ecological Engineering, Korea University, Seoul 02841, Republic of Korea; [2]EMBIOME, Seoho-ro, Gwonseon-gu, Suwon, Gyeonggi 16614, Republic of Korea.

***Correspondence:** Woojun Park, wpark@korea.ac.kr

Keywords: biofilm; CpG island; *Deinococcus*; extracellular matrix; genome deletion; stress response.

Abbreviations: CLSM, confocal laser scanning microscopy; DAPI, 4′,6-diamidino-2-phenyl indole; ECM, extracellular matrix; EPS, exopolysaccharide; GS, glyoxylate shunt; HPEAC, high-performance anion-exchange chromatography; LPS, lipopolysaccharide; PCR, polymerase chain reaction; PI, propidium iodide; RDR, radiation and desiccation response; TCA cycle, tricarboxylic acid cycle; TYG, Tryptone-yeast extract-glucose; WT, wild-type.

Data statement: All supporting data, code and protocols have been provided within the article or through supplementary data files. Eight supplementary figures and eleven supplementary tables are available with the online version of this article.

the architecture of their biofilms, and their potential bioremediation applications have been studied previously [10–12]. However, the molecular mechanisms of biofilm formation, the types of EPSs and proteins in the ECM, and the genes associated with EPS synthesis in these species remain unknown. Because of their high capacity for DNA repair and biofilm formation, *Deinococcus* spp. are ubiquitous and interact with diverse micro-organisms via the production of biofilm in both natural and artificial environments; however, only minor *Deinococcus* populations have been characterized due to their slower growth compared to other bacteria [13, 14]. Interestingly, *Deinococcus* spp. are commonly detected in the evaporator cores of air-conditioning systems, although their proportion varies among samples from different countries [15]. For instance, four *Deinococcus* species (*Deinococcus aluminii*, *Deinococcus multiflagellatus*, *Deinococcus metallilatus* and *Deinococcus carri*) were isolated from automobile air-conditioning systems, and their biochemical activities and bacterial phenotypes were analysed [16–18]. However, a comprehensive analysis of *Deinococcus* species isolated from air-conditioning systems has not been conducted.

D. metallilatus (i.e. the bacterial species studied here) is phylogenetically closer to *Deinococcus geothermalis* than *D. radiodurans* and exhibits optimal growth at 40 °C (*D. radiodurans*, 32 °C; *D. geothermalis*, 50 °C) [18, 19]. Genetically modified *D. geothermalis* strains have been demonstrated to reduce Cr(VI) at 40 °C, suggesting that this recombinant strain can be used for bioremediation under high temperature and in radioactive waste-polluted environments [20]. Therefore, *D. metallilatus* would be also well-suited for heavy metal bioremediation research in high-temperature environments. Moreover, enhanced biofilm formation capacity of *D. metallilatus* would lead to a more stable bacterial growth under stress conditions. Recent research has demonstrated that uranium was effectively reduced using a biofilm-overproducing *D. radiodurans* R1 strain (DR1-bf^{+}) [12]. Additionally, the biofilm formation capacity of *Deinococcus* spp. has not been well characterized via molecular approaches, and therefore the development of a *D. metallilatus* biofilm overproduction strain would aid in the characterization of the molecular mechanisms of deinococcal biofilm formation.

Here, biofilm-overproducing mutants were generated via UV-induced mutagenesis, after which physiological examinations were conducted. Moreover, based on genomic and transcriptomic analyses of wild-type (WT) and mutant bacteria, a mechanistic model of biofilm enhancement in mutant strains was proposed.

Impact Statement

Deinoccocus spp. are well known multi-stress-resistant bacteria due to their genomic contents and plasticity. However, genomic analyses after ultraviolet irradiation have yet to be comprehensively conducted. Furthermore, the mechanisms of biofilm formation that contribute to multiple stress resistance have yet to be established in *Deinococcus* spp. Therefore, this study sought to compare the genomes of wild-type and biofilm-overproducing *Deinococcus metallilatus* strains. Interestingly, biofilm-overproducing cells exhibited large genome deletions and fragmentation within the CpG islands of a secondary chromosome. Furthermore, transcriptomic analyses revealed that the aforementioned deletions resulted in growth defects under glucose metabolism, which promotes biofilm formation by increasing exopolysaccharide synthesis.

METHODS

Bacterial strains, reagents and growth conditions

D. metallilatus MA1002, which was isolated from an automobile air-conditioning evaporator, was identified as a novel species in a previous study and was used here [18]. UV mutagenesis was performed as illustrated in Fig. S1a (available in the online version of this article). Briefly, resuspended cells (OD_{600}=1.0) were irradiated using a UV crosslinker (UVP CL-1000, USA) under 25 mJ cm^{-2} of UV intensity for 90 s. After irradiation, diluted samples (10^{-2}, 10^{-3} and 10^{-4}) were plated onto tryptone yeast extract glucose (TYG) agar. After a 48 h cultivation period, the colonies were transferred to 96-well plates containing TYG media for screening.

The aerobic growth of *D. metallilatus* WT strain and mutant strains no. 5 and no. 6 was determined via optical density (OD_{600}) measurement of cultures at 30 °C and 220 r.p.m. using a Biophotometer (Eppendorf, Germany). The cells were initially washed twice with phosphate-buffered saline (PBS) and inoculated into a 50 ml flask containing 20 ml of TYG medium [3 g l^{-1} tryptone (Bioshop, Canada), 3 g l^{-1} yeast extract (Bioshop, Canada), 3 g l^{-1} D-glucose (Junsei, Japan), and 1 g l^{-1} K_2HPO_4 (Junsei, Japan)]. The final optical density of the inoculates was then adjusted to an OD_{600} of approximately 0.04. To observe the growth of WT and mutant strains under static conditions, 200 µl of TY medium including cells (OD_{600}, ~0.04) were aliquoted into each well in 96-well microplate (BD Biosciences, USA). If required, 16.8 mM glucose, sodium acetate (NaAc) and sodium glyoxylate (NaGox) were added to the TY medium. Cell growth was measured at 1 h intervals for 100 s with constant shaking using a Spark microplate reader (Tecan, Switzerland). The MA1002 strain was deposited in the Korea Collection for Type Cultures (accession number, KCTC 17964).

Confocal laser scanning microscopy and fluorescence microscopy

Biofilm cells were visualized via FilmTracer SYPRO Ruby biofilm matrix staining for 30 min at room temperature and observed through confocal laser scanning microscopy (CLSM; Carl Zeiss, Germany). Confocal images of stained biofilms were observed under red fluorescent light (excitation wavelength, 450 nm; emission wavelength, 610 nm) to evaluate the height and density of the biofilm. The cells were then cultured

for 24 h and stained with 4′,6-diamidino-2-phenylindole (DAPI; 40 µg ml^{-1}) or FM4-64 (50 µg ml^{-1}) to visualize their DNA and cell membranes, respectively. After 10 min of incubation at room temperature, the samples were mixed with TYG 2× agarose and loaded onto glass slides. Microscopic analyses were conducted using a fluorescence microscope (Carl Zeiss, Germany) equipped with 365 and 550 nm wavelength excitation filters.

Biofilm formation quantification

Biofilm formation quantification was carried out as described previously [21]. Briefly, the plates were incubated at 30 °C without agitation. The microtitre plates were then rinsed twice with sterile deionized water (DW), and the remaining attached cells were stained with a 0.1% (w/v) crystal violet (CV) solution for 30 min. The CV solution was then removed, and the wells were rinsed with DW. The absorbance of the dye dissolved in 95% ethanol was measured at 595 nm (OD_{595}), which was normalized to OD_{600}.

ECM extraction and quantification

Twenty-four, 48 and 72 h WT and mutant strain cultures were centrifuged (1 min at 13200 r.p.m.), after which the supernatant was discarded. Cell pellets were then resuspended in 1.5 M NaCl, as described previously [22]. The resuspended cells were then centrifuged once more, and the supernatant was collected to measure the concentration of DNA, proteins and saccharides. To quantify DNA in the isolated ECM, DNA was purified with the Promega SV Wizard DNA purification system (Promega, USA) according to the manufacturer's instructions. The concentration of the purified DNA was measured using an Implen N60 nano-spectrophotometer (Implen, USA). Proteins in the isolated ECM fractions were quantified via the Bradford assay based on a bovine serum albumin standard curve. Protein concentration was measured at 590 nm on a UV/Vis spectrophotometer (Eppendorf, Germany). The total saccharide concentration in the ECMs was measured using the phenol–sulfuric acid method [22]. Briefly, 20 µl of 5% phenol was added to 20 µl of the ECM fraction and mixed in the 96-well plate. Afterward, 100 µl of sulfuric acid was added, and the mixture was incubated for 10 min at room temperature. Saccharide concentration measurements were performed at 492 nm using a Spark (Tecan, Switzerland) instrument with glucose as a standard.

EPS purification and HPAEC analysis

EPS was extracted via ethanol precipitation [23]. Cells were incubated in 1 l of TYG medium for 72 h and centrifuged to obtain a clear supernatant, followed by the addition of three volumes of ethanol and incubation overnight at 4 °C. The samples were then centrifuged and the pellets were washed three times with an 80% ethanol solution, followed by three washes with PBS to remove debris and freeze-drying for 3 days. The freeze-dried EPS samples were then analysed via high-performance anion-exchange chromatography (HPAEC; ICS-5000, Dionex Co., USA). A CarboPac PA-1 (Dionex Co., USA) column was used with 18 mM NaOH as the solvent at a flow rate of 1.0 ml min^{-1} at 25 °C. HPAEC was performed by Biosystems, Republic of Korea.

Genome sequencing and comparative genome analysis

The genomic DNA of *D. metallilatus* was extracted using a Wizard DNA purification kit (Promega), and genome sequencing was conducted using a PacBio 20K sequencer for the WT strain and a MiSeq sequencer (paired-end libraries) for the mutant strain at Chunlab (Seoul, Republic of Korea). *De novo* assembly of the quality-filtered sequencing reads obtained from the WT strain was conducted using PacBio SMRT Analysis 2.3.0 software. The genome sequence of the *D. metallilatus* MA1002 WT strain can be accessed through the GenBank database (accession nos CP038510–CP038512 for WT, VBRC00000000 for no. 5 mutant and SDEC00000000 for no. 6 mutant). The read mapping results were visualized using Artemis (https://www.sanger.ac.uk/science/tools/artemis). Genskew (http://genskew.csb.univie.ac.at/) was used to calculate the normal and cumulative GC skew of the MA1002 genome, whereas the origin of replication (*oriC*) site and DnaA box clusters were determined using the OriC finder web tool (http://origin.tubic.org/Ori-Finder/). A total of 40 and 151 contigs from the genome sequences of strains nos 5 and 6, respectively, were aligned to the genome of the WT strain (which was used as the reference) using Mauve software (http://darlinglab.org/mauve/mauve.html). A dot plot analysis was performed using D-GENIES (http://dgenies.toulouse.inra.fr/). DBCAT (http://dbcat.cgm.ntu.edu.tw/) was used to search for CpG islands in the MA1002 genome using the default parameters. A BLAST Atlas search was performed to compare coding sequences (CDSs) between the WT and mutant genomes using the Gview server (https://server.gview.ca/).

RNA isolation and transcriptomic analysis via RNA-seq

WT and mutant strain cells were harvested after 24 h of incubation (exponential phase, Fig. 1d) at 220 r.p.m. and 30 °C. Total RNA was isolated from 10 ml of cells using the RNeasy Mini kit (Qiagen, USA) according to the manufacturer's instructions. RNA was subjected to subtractive Hyb-based rRNA removal using the MICROB Express Bacterial mRNA Enrichment kit (Ambion, USA). A library was constructed as described previously [24]. RNA sequencing was performed in two runs using the Illumina Genome Analyzer IIx system to generate single-ended 100 bp reads. Quality-filtered reads were aligned to the reference genome sequence using CLC Genomics Workbench 6.5.1 software (CLC bio, USA). Mapping was based on a minimal length of 100 bp with an allowance of up to two mismatches. The relative transcript abundance was measured in RPKM. All procedures used for RNA sequencing were carried out at Chunlab (Republic of Korea). All RNA-seq data were deposited in the National Center for Biotechnology Information (NCBI) database under the Gene Expression Omnibus accession number GSE130360.

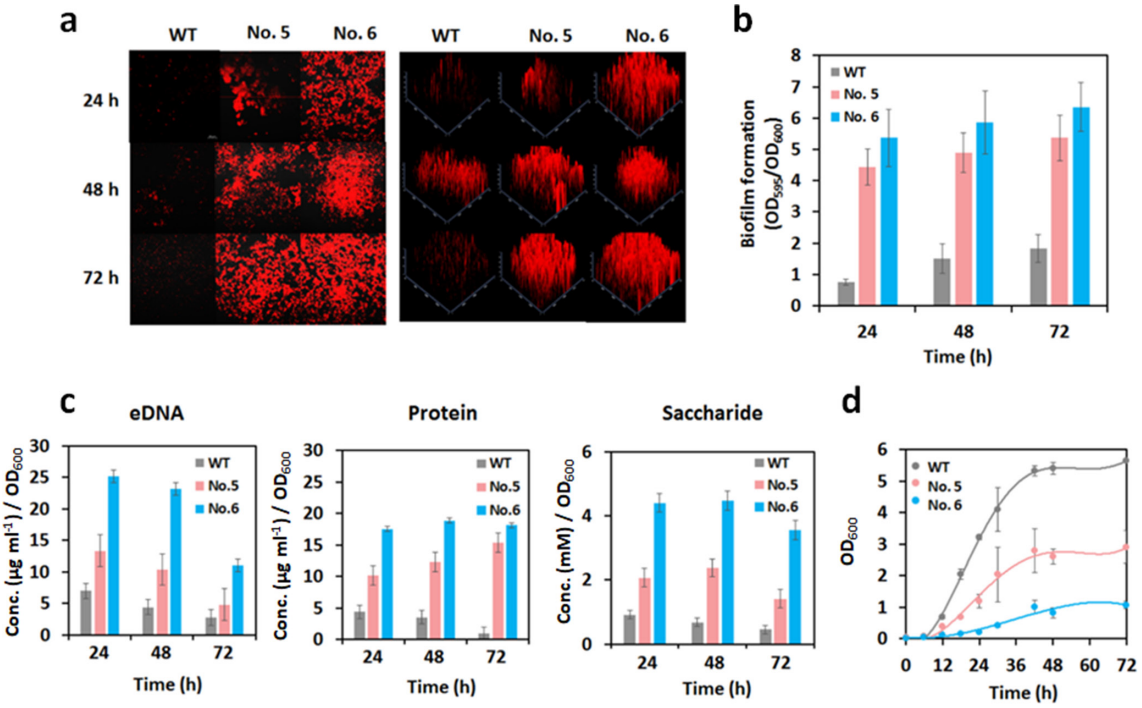

Fig. 1. Growth and biofilm formation of WT and mutant strains. (a) Confocal laser scanning microscopy image analysis of biofilm. Biofilm was stained with the Film Tracer Ruby staining dye for 30 min, then observed in each strain at 24, 48, and 72 h based on two differential (left) and three differential (right) images. (b) Quantification of biofilm formation using the crystal violet-staining method. All biofilm assays were performed using five replications. (c) Examination of ECM components (eDNA, proteins, and saccharides). All components were evaluated in triplicate and measured at 24, 48, and 72 h. (d) Growth tests of the WT (grey line) and mutant (no. 5: pink line, no. 6: blue line) strains in 20 ml of TYG medium with agitation. The graphs show the average of duplicate experiments and the error bars indicate the standard deviation.

Flow cytometry analyses

Samples were cultured with or without agitation in 16.8 mM glucose-, NaAc- and NaGox-supplemented TY medium for 24 h, followed by 1/2 dilution with PBS for cell counting. After the addition of 20 mM PI to 500 µl sample dilutions, the samples were vortexed and incubated for 1 min on ice. Stained cells were measured using a portable flow cytometer (BD Accuri C6 Plus). The threshold conditions were fixed at 8000 cells, and a total of 500000 cells were analysed in each experiment.

PCR

To confirm whether contigs were independent, PCR was conducted using contig 1, contig 2 and contig 3 forward (F) and reverse (R) primers designed from the ends of each contig (Table S1). Additionally, PCR was performed to confirm the occurrence of *eda* genes (*eda*1 and *eda*2) in WT and mutant strains using *eda*-specific primers (Table S1). All PCR procedures were performed using a KAPA HiFi PCR kit (KAPA Biosystems, USA) with the following cycling conditions: 35 cycles of 45 s at 95 °C for denaturation, 45 s at 60 °C for annealing and 45 s at 75 °C for elongation.

qRT–PCR

cDNA synthesized from 1 µg of each RNA was used as a template. The PCR mixture contained 1 µl of 0.5 µm forward and reverse primers (Table S1) and 2 µl of 100-fold diluted cDNA, 10 µl of Power SYBR Green PCR Master Mix (Applied Biosystems, USA) and 6 µl of DW in a total volume of 20 µl. The PCR conditions were set at 48 °C for 30 min and 95 °C for 10 min for the first holding stage, followed by 42 cycles of 15 s at 95 °C for the cycling stage and 15 s at 95 °C, 1 min at 60 °C and again 15 s at 95 °C for the melting curve stage. The expression of each gene was normalized to that of the 16S rDNA gene. The quantification results were based on triplicate samples.

Protease activity quantification

WT and mutant cells growing in 50 ml of TYG medium were harvested at 24 h by centrifugation (7860 r.p.m. for 10 min), after which the supernatants were removed. Cell pellets were washed twice with PBS, and the resuspended cells were lysed by sonication. After centrifugation, the supernatants were collected and used for protease activity quantification. Casein (0.04 g) was added to 2 ml of potassium phosphate buffer (pH 8), and a 500 µl sample was transferred to the casein mixture, followed by incubation with shaking for 1 h.

After the enzymatic reaction, 2.5 ml of 1.2 M trichloroacetic acid (TCA) was added to the mixture, followed by centrifugation. The supernatant of the mixture was transferred to 0.5 N Ciocalteu solution and treated with 5 ml of Na_2CO_3 (0.4 M). The sample was then measured using a UV/Vis spectrophotometer at 660 nm; tyrosine was used to construct the standard curve.

RESULTS

Generation of biofilm-overproducing mutants via UV-induced mutagenesis

For random mutagenesis, it is necessary to determine the appropriate UV intensity for the generation of mutants. Thus, the UV resistance of *D. metallilatus* was examined. Cell density was reduced by approximately 100-fold when irradiated with 5 mJ cm^{-2} of UV for 60 s. However, there was no significant cell mortality after exposure to UV radiation up to 30 mJ cm^{-2} for 60 s, indicating that a 60 s irradiation induces cellular stress but is insufficient to generate mutants due to high cell viability (Fig. S1b). A significant decrease in cell density (i.e. by approximately 10^4-fold) was observed at 25 mJ cm^{-2} for 90 s (Fig. S1a), and a 120 s irradiation yielded an extreme reduction in cell density, even at 5 mJ cm^{-2} (10^5-fold reduction). Therefore, the appropriate UV intensity and irradiation time for UV mutagenesis were determined to be 25 mJ cm^{-2} for 90 s. UV-induced random mutagenesis was performed using these parameters, as shown in Fig. S1a and as described in the Methods section. Forty-nine candidates were considered to be biofilm-overproducing strains during the preliminary screening, and eight strains were randomly selected for the secondary screening (Fig. S1c). After the secondary screening, strain nos 5 and 6 exhibited the highest biofilm-formation capacity among all candidates. Furthermore, a high degree of biofilm production in mutant strain no. 6 was possibly observed during bacterial culture (Fig. S1d). Thus, strain nos 5 and 6 were selected for further biofilm overproduction analyses.

Biofilm formation and growth of WT and mutant strains

Image analysis using CLSM revealed that the mutants produced a larger amount of biofilm than the WT at all time points examined herein (24, 48 and 72 h) (Fig. 1a). The quantification of biofilm production indicated that mutant strain no. 5 formed biofilm at a rate that was 5.8-, 3.3- and 2.9-fold higher than that of the WT strain at 24, 48 and 72 h, respectively. At the same time points, strain no. 6 also formed large amounts of biofilm (7.1-, 3.9- and 3.5-fold changes vs the WT strain); however, the amount of biofilm produced by the three strains did not increase significantly over time (Fig. 1b). The concentration of eDNA, protein and saccharide (i.e. ECM components) in both mutants was higher than that of WT bacteria, which was consistent with the results of the biofilm assay (Fig. 1b, c). However, all ECM components of the parent strain were slightly decreased over time, whereas those of the mutants were maintained up to 48 h. The concentration of eDNA in the ECM of both mutants was the highest at 24 h but was significantly decreased at 72 h (Fig. 1c). However, saccharide concentration was slightly decreased in the mutants after the concentration of proteins in the ECM was maintained or even increased at the aforementioned time point (Fig. 1c). To further analyse the biofilm saccharide composition, a high-performance anion-exchange chromatography (HPAEC) analysis of EPS was performed. Among the monosaccharides assessed (rhamnose, arabinose, galactose, glucose, mannose, xylose, fucose and fructose), only four types (mannose, glucose, galactose and fucose) were detected in WT EPS (Table S2). Mannose and glucose were commonly detected and were the predominant monosaccharides in EPS secreted by the WT, no. 5, and no. 6 strains. Moreover, galactose was detected in the EPS of the WT and no. 5 strains, and a low amount of fucose was detected only in WT EPS (Table S2).

It is generally believed that bacteria form biofilm under stressful conditions [25]; thus, biofilm-overproducing mutants might exhibit slow growth to compensate for this high biofilm formation ability. A parent strain started to grow at 12 h and reached the stationary phase within 48 h. A similar pattern was observed for mutant strain nos 5 and 6 (Fig. 1d). However, the maximum OD_{600} value of the WT strain at 72 h was >5.6, whereas those of strains nos 5 and 6 were 2.9 and 1.0, respectively, indicating that the mutants had severe growth defects (Fig. 1d). Therefore, the mutant strains exhibited a trade-off between growth and biofilm production.

Genomic sequencing analysis of *D. metallilatus* MA1002

Genome sequencing was performed to compare WT and mutant strains at the genome level. However, the reference genome (WT) was analysed prior to comparative genome analysis. Table S3 summarizes the results of whole-genome sequencing. Among a total of three contigs, contig 3 exhibited the largest genome size (3062036 bp), followed by contig 1 (876461 bp) and contig 2 (408147 bp). Additionally, contigs 3 and 1 carried nine and three rRNA genes, respectively, whereas no rRNA genes were present in contig 2. tRNA genes were only present in contig 3 (49 genes). The read mapping data indicated gaps between each contig (Fig. S2a). Therefore, polymerase chain reaction (PCR) was used to confirm whether all contigs were independent of each other (Fig. S2b). The expected fragment size based on the terminal primer for each contig amplified (109, 154 and 126 bp) indicated that *D. metallilatus* MA1002 harbours three independent replicons (Fig. S2b).

Because contig 3 (1254609–4346644 bp) was considered to be the main chromosome based on genome sequencing profiles (contig size and the number of rRNA and tRNA genes), further analyses were performed to identify the origin of replication (*oriC*) and termination (*ter*) sites in this contig. The cumulative GC skew data of the genome showed that the lowest cumulative GC skew index (−1.351) was located at 2868361 bp, whereas the highest index value (1.44) was located at 4254735 bp (Fig. S3a). Furthermore, DnaA box

clusters were largely detected at 1286052–1286241 and 4286060–4286266 bp (Fig. S3b), indicating that an *oriC* site was present at the start and end sites of contig 3, whereas a *ter* site was located at 2868361 bp. However, contig 1 (1–876461 bp) and contig 2 (876462–1254608 bp) did not show any observable characteristics of cumulative GC skew or DnaA box cluster profiles (Fig. S3a, b). Genes encoding plasmid partition proteins (*parA* and *parB*) and replication proteins [*repA* (or *repB*)] were located together within contig 1 [*parA*, 13974–14750 bp; *parB*, 13099–13977 bp; and *repA* (or *repB*), 15502–16905 bp]. Furthermore, the expected DnaA box (TCTCCCACAT) and RepA box (AGACAGCAA) were detected between the *parA* and *repA* genes (14751–15502 bp) (Fig. S3c). In this non-coding region, eight direct repeats (ACAACTTGCGCC) and two palindromic sequences (TGTTGACAACA and TCTTTTAAAAGA) were present within the AT-rich region (Fig. S3c). In summary, genomic sequencing analyses revealed that *D. metallilatus* harboured three replicons, of which contig 3, contig 1 and contig 2 will be henceforth referred to as the main chromosome, secondary chromosome and megaplasmid, respectively.

Comparative genome analysis of WT and mutant strains

Genomic sequencing of the two mutant strains was conducted using a MiSeq sequencer, and reads were mapped based on the reference genome (WT). In total, 40 and 151 contigs were derived from the genomes of strain nos 5 and 6, respectively. Typically, 33 contigs from both mutants matched with the main chromosome, and 1 contig from the mutants belonged to the megaplasmid of the parental strain (Table S4). However, only 3 contigs in strain no. 5 aligned to the secondary chromosome, whereas 25 contigs matched to the secondary chromosome in strain no. 6. Three and 92 unmatched contigs were present in strain nos 5 and 6, respectively (Table S4). The whole-genome size of the WT, no. 5, and no. 6 strains was 4346644, 4098227 and 4025657 bp, indicating that genomic deletion occurred in the two mutants. Furthermore, both dot plot analysis and Mauve alignment suggested that the regions corresponding to 271101–575926 and 336652–771258 bp were not present in the genome of strain nos 5 and 6, respectively (Fig. S4a, b). Interestingly, the nucleotide sequences of the 271089–271100 and 575927–575938 bp regions in the WT genome overlapped, which was related to the 417918–417929 bp DNA sequence in the genome of strain no. 5. Furthermore, two nucleotide sequences (333058–333652 and 771669–772293 bp) were the same in the WT genome, but only one sequence was found in the genome of strain no. 6, suggesting that the deletion site was present within the overlapped sequences (Fig. S5). However, the mapping of contigs from mutants to a reference chromosome or plasmid did not suggest the detection of any noticeable characteristics (Fig. S6), which was supported by dot plot and Mauve alignment analyses (Fig. S4a, b).

It is well known that methyl CpG islands in animal cells are preferentially targeted by UV irradiation, forming cyclobutane pyrimidine dimers or inducing double-stranded breaks; however, these structures have not been analysed in bacteria [26, 27]. Examination of CpG island regions in the genome of *D. metallilatus* MA1002 elucidated the presence of five CpG islands (>200 bp) in the secondary chromosome, which had a 67.6% average GC content. Specifically, the five CpG islands (138129–405172; 405398–423132; 423312–470451; 470628–478458; 479066–876429 bp) exhibited a 67, 59, 62, 57, and 68% GC content, respectively (Fig. 2a). Moreover, a highly dense GC content was observed in the 479089–480000 bp region of the secondary chromosome (GC content, 70%). The deleted regions in the genome of strain nos 5 and 6 belonged to the CpG islands (Fig. 2a), and several DNA fragments of CDSs (80–90% identity) were present in these deleted regions (Fig. 2b). In conclusion, large genomic deletions and fragmentations occurred in the secondary chromosome of the mutant strains, and CpG islands were hotspots for genomic modification under UV stress.

Expression of genes related to carbohydrate metabolism and EPS/lipopolysaccharide (LPS) synthesis in mutants

It was thought that the biofilm overproduction was likely linked to a common deleted site in the genomes of both mutants (strain nos 5 and 6). A total of 198 genes in the secondary chromosome were included in this common deletion region (336652–575926 bp), the expression of which was almost impaired. Among these genes, we focused on genes that were expressed in the WT strain and exhibited a high number of reads per kilobase of transcript (RPKM, >100; n=14 genes). Four carbohydrate metabolism-related genes were found to be deleted among the 14 genes in the mutant strains [alpha-galactosidase (*gla*), glucosamine-fructose-6-phosphate aminotransferase (*glmS*), *N*-acetylglucosamine-6-phosphate deacetylase (*nagA*) and UDP-*N*-acetyl glucosamine-undecaprenyl-phosphate *N*-acetyl glucosamine phosphotransferase (*wecA*)] (Table S5). Further analysis suggested that several genes participating in glucosamine and gluconate metabolism were deleted in the mutant strains. However, *D. metallilatus* possesses several homologous genes that might replace the function of deleted genes, except for the gene encoding *N*-acylglucosamine-6-phosphate-2-epimerase (*nagC*). Furthermore, two copies of genes encoding 2-dehydro-3-deoxy-phosphogluconate (KDPG) aldolase (*eda1* and *eda2*) were absent in the mutant genomes (Fig. 3, Table S6), which was confirmed by PCR (Fig. S7a).

The RNA-seq data suggested that most genes related to the glycolysis pathway were constitutively expressed; however, the *fbaA*, *gapA* and *pgk* genes were slightly upregulated in the mutant no. 6 strain compared with those in the parental strain (*fbaA*, 1.7-fold; *gapA*, 1.3-fold; *pgk*, 1.4-fold) (Fig. 3, Table S7). In contrast, the expression of genes that participate in the Entner–Doudoroff (ED) and pentose phosphate (PP) pathways was significantly decreased (*gdh*, 0.5-fold; *zwf*, 0.6-fold; *edd*, 0.5-fold; *pgl*, 0.8-fold; *gnd*, 0.6-fold; *rpiA*, 0.4-fold) (Fig. 3, Table S8). The expression of genes of the mannose

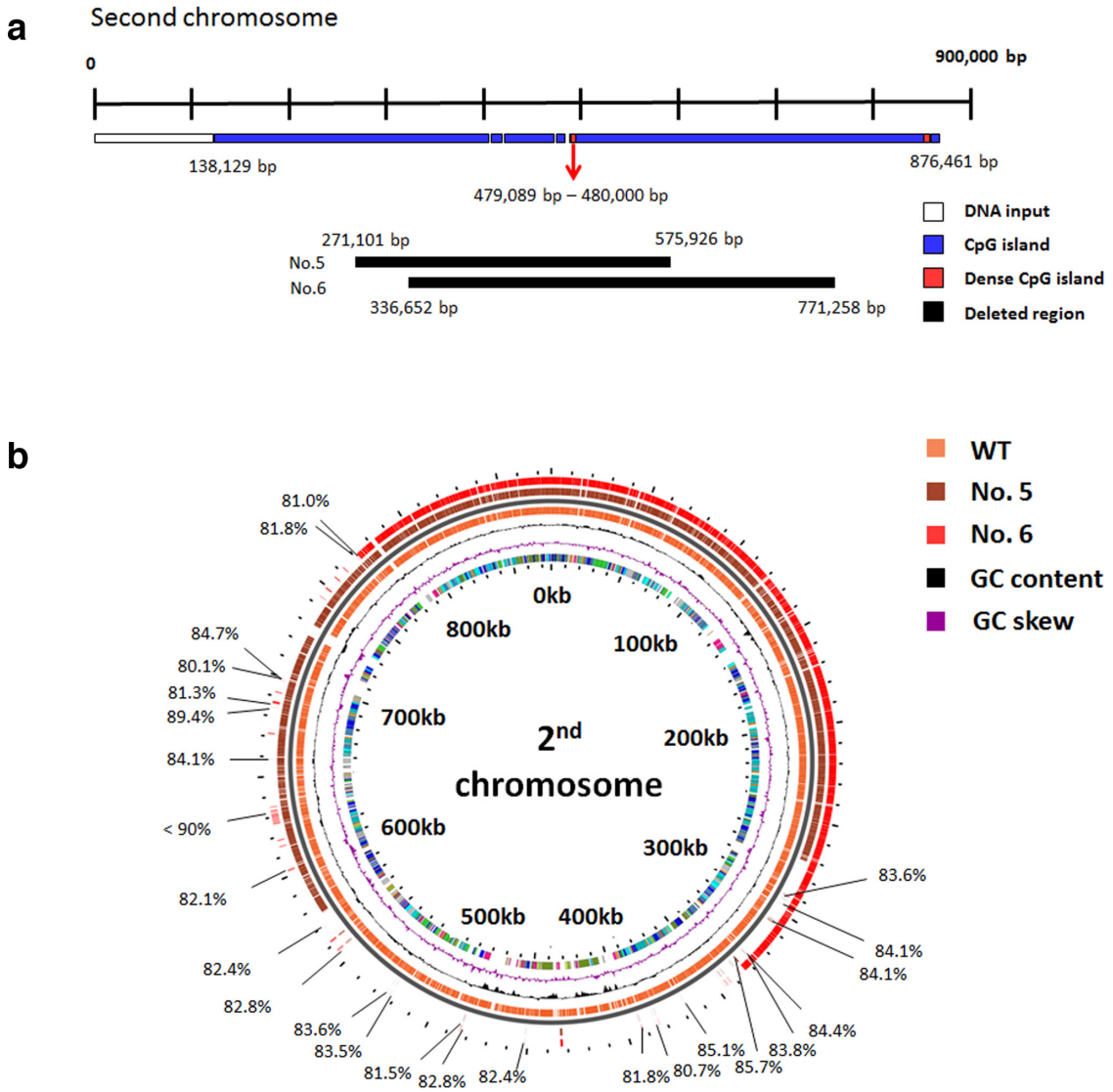

Fig. 2. Description of genome deletion and fragmentation in a secondary chromosome of WT and mutant strains. (a) Schematic representation of the CpG islands in a secondary chromosome of *D. metallilatus* MA1002 (876461 bp). Within the entire DNA input (white horizontal box), normal and dense CpG islands are indicated in blue and red, respectively (138129–772293 bp). The black horizontal box represents the deleted region in the genomes of strain nos 5 and 6. (b) Comparative genome analysis using BLAST Atlas. Gview server (http://server.gview.ca) was used to map CDSs to the genomes of WT (orange), no. 5 (brown) and no. 6 (red) strains. The percentages indicate the similarity of CDSs between the WT and mutant genomes.

and galactose metabolism pathway, which produces GDP-mannose, UDP-glucose and UDP-galactose, was not significantly induced in the mutant no. 6 strain. Moreover, although the *glmS* gene (which encodes glucosamine-fructose-6-phosphate aminotransferase) was upregulated by 2.3-fold in the mutant no. 6 strain, unlike the WT strain, downstream genes related to the aminosugar synthesis pathway were expressed constitutively (Fig. 3, Table S7). We also confirmed the upregulation of *glmS*, the constitutive expression of *manB* and the downregulation of *zwf* in the nos 5 and 6 mutant strains using quantitative reverse transcription PCR (qRT–PCR) (Fig. 3b).

D. metallilatus possesses one major operon for predicted EPS/LPS synthesis in the main and secondary chromosomes. The expression of the EPS synthesis operon in the main chromosome was increased in the mutants; in particular, the *wzx*, *glfT*, *espF*, *wzy*, *rfaB*, *glgA*, *wcaG* and *wcaJ* genes were upregulated by at least 1.5-fold (Table S8). qRT–PCR also determined that the expression of the *galE*, *espF*, *rfaB* and *glgA* genes was increased by >1.6-fold in mutant no. 6 compared with that in the WT (Fig. 3b). However, a relatively low induction was detected in mutant no. 5 (*galE*, 1.6±0.1-fold; *epsF*, 1.2±0.1-fold; *rfaB*, 1.2±0.1-fold; *P*-value <0.05) (Fig. 3b). Conversely, the LPS

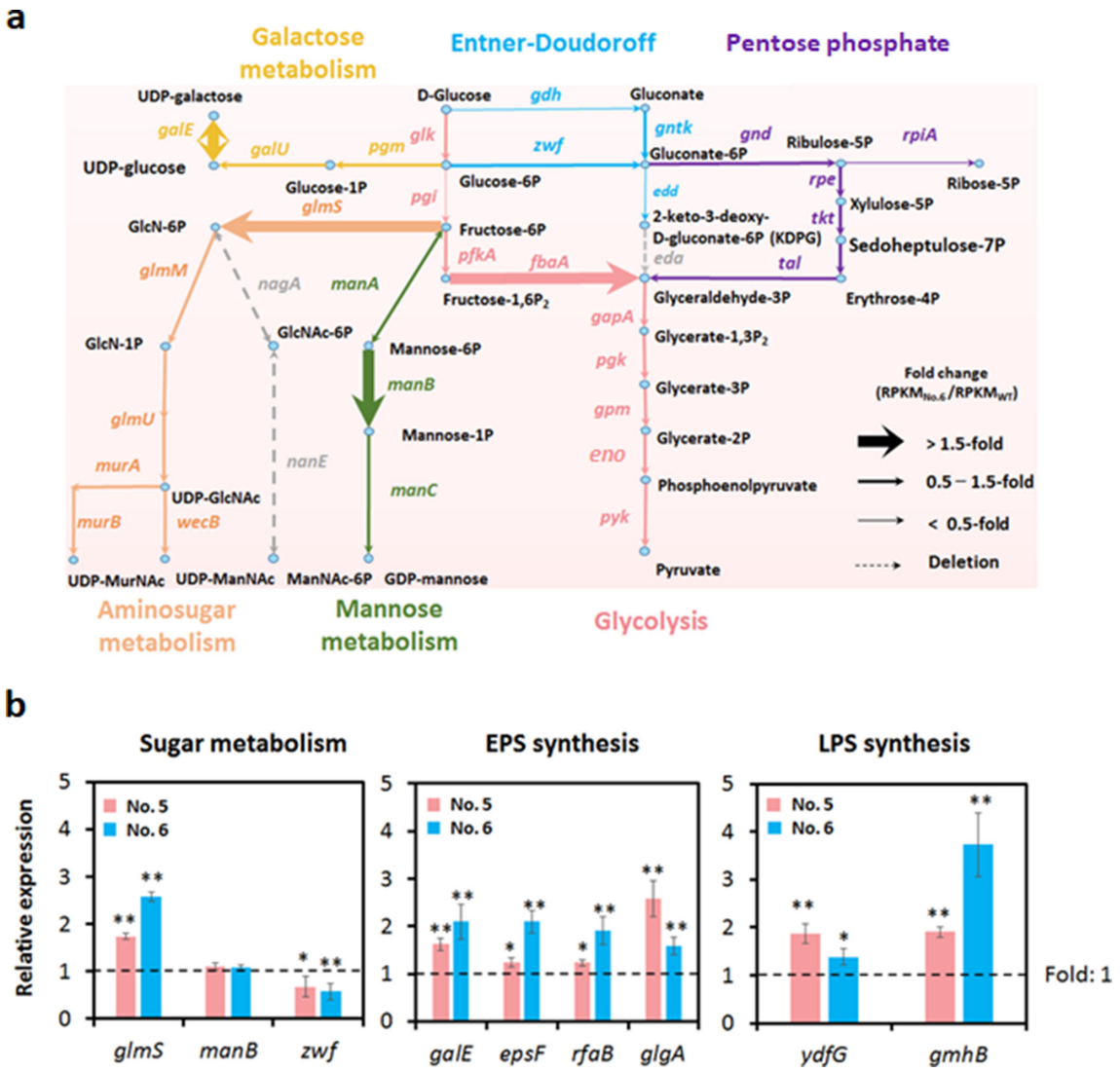

Fig. 3. Gene expression profiles of sugar metabolism and EPS/LPS synthesis. (a) Schematic representation of the sugar metabolism pathway and gene expression analysis results. The thickness of the arrows indicates the expression fold change (RPKM $_{no.\ 6}$/RPKM $_{WT}$), and the dotted grey arrows represent deleted genes in the mutants. (b) Relative expression of genes that participate in sugar metabolism (*glmS*, *manB* and *zwf*), EPS synthesis (*galE*, *epsF*, *rfaB* and *glgA*) and LPS synthesis (*ydfG* and *gmhB*) in mutants compared with the WT strain. All data are reported as the average of triplicate experiments, and the error bars indicate the standard deviation. A *t*-test was performed between the WT and each mutant strain (**P* <0.05; ***P* <0.01). The black horizontal dotted line represents a onefold change in expression, which is the relative expression level of the WT strain.

synthesis-related gene cluster located in the secondary chromosome was not significantly increased. Although the expression of the *adeR*, *ydfG*, *gmhB*, *gmhC* and *waaF* genes was induced by >1.3-fold (RNA-seq expression: Table S8; qRT–PCR expression: 1.4±0.2-fold for *ydfG* and 3.7±0.7-fold for *gmhB*; *P*-value <0.05, Fig. 3b) in the no. 6 strain, the genes encoding hexosyltransferases (*rfaQ* and *rfaF*), trehalose synthase (*rfaB*) and glycosyltransferase (*gmhA*) in this operon were downregulated in the no. 6 mutant genome (Table S8). In conclusion, upregulation of genes related to glycolysis and EPS synthesis and downregulation of genes participating in the PP and ED pathways were observed in the mutant strains. Furthermore, two *eda* genes were completely absent from the mutant genome.

Evidence of damaged cells in a mutant strain grown in TYG medium

The severe growth inhibition and the large genomic deletions observed in the mutants suggest that mutant strains undergo stress during growth, leading to the induction of stress response-related genes. Based on previous studies [28], *D. radiodurans* stress response genes were searched in the genome of *D. metallilatus* MA1002 by focusing on

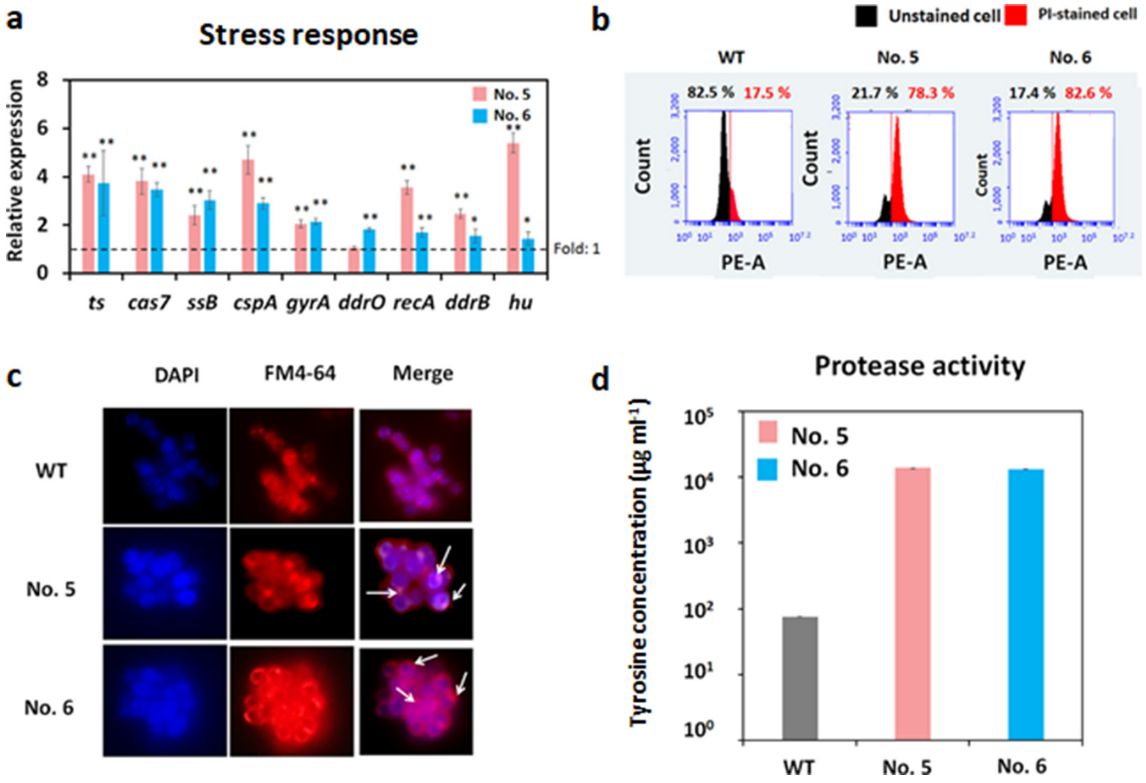

Fig. 4. Evaluation of dead cell counts and evidence supporting cell death. (a) The relative expression of stress response genes in mutants was evaluated by comparison with that in the WT strain using qRT–PCR. All data are reported as the average of three replicates, and the error bars indicate the standard deviation. A *t*-test was performed between the WT and each mutant strain (**P* <0.05; ***P* <0.01). The black horizontal dotted line represents a onefold change in expression, which is the relative expression level of the WT strain. (b) Flow cytometric analysis of PI-stained (red) and non-stained (black) cells in TYG medium after 24 h of cultivation with agitation. The *x*- and *y*-axes represent PE-A (fluorescence intensity) and cell counts, respectively. (c) DIC microscopic image analysis. DNA and membranes (vesicles) were stained with the DAPI and FM4-64 dyes, respectively. The white arrows indicate predicted vesicles (1000× magnification). (d) Measurement of protease activity in the WT, no. 5 and no. 6 strains. The *y*-axis represents the concentration of tyrosine, which is a product of casein degradation. Samples were measured in duplicate, and the average is reported.

upregulated genes with RPKM >100 (Table S9). RNA-seq data suggested that the expression of protein RecA (*recA*), DNA damage response B (*ddrB*), single-stranded DNA-binding (*ssb*) and HTH-type transcriptional regulator DdrOC (*ddrO*) homologous genes, which are known as the radiation and desiccation response (RDR) genes, was increased in the mutant no. 6 strain by 1.3-, 1.4-, 1.9- and 1.3-fold, respectively (qRT-PCR: 1.7±0.1-, 1.6±0.2-, 3.0±0.4- and 1.8±0.1-fold; *P* <0.05). Furthermore, this upregulation was also observed in mutant no. 5 (qRT-PCR: 3.6±0.3-, 2.5±0.2-, 2.4±0.4- and 1.0±0.1-fold; *P* <0.05). The *gyrA* and *gyrB* genes, which encode DNA gyrases, were upregulated by >1.3-fold (Table S9). Two genes encoding histone-like proteins (*hu1* and *hu2*) were upregulated by >1.5-fold in mutant no. 6 compared with those in the WT strain. Although the expression of GroEL/ES chaperone-encoding genes was not significantly increased in the mutant (~1.1-fold), genes for cold-shock proteins (*cspA*, 1.6-fold; *cspB*, 1.3-fold), which stabilize DNA and RNA molecules under stress, and for the transcription elongation factors Ts/Tu (*ts*, 2.4-fold; *tu1*, 1.6-fold; *tu2*, 2.0-fold), which function as chaperones during protein stabilization, were induced in mutant no. 6 (Table S9). The CRISPR/Cas system is a defence mechanism of adaptive immunity in bacteria and archaea against phages and plasmids. In the genome of *D. metallilatus*, two CRISPR/Cas operons were located in the main and the secondary chromosomes, respectively. Both operons were expressed at a level that was at least 1.7-fold higher in the no. 6 mutant than in the WT (Table S9). Among the stress response genes mentioned above, nine representative genes (*ts*, *cas7*, *ssb*, *cspA*, *gyrA*, *ddrO*, *recA*,*ddrB* and *hu*) that were highly induced in no. 6 mutant strain were chosen and qRT–PCR was performed. Although the *ddrO* gene was not induced in mutant no. 5, most of these genes were induced by >1.4-fold in both mutants (Fig. 4).

To demonstrate the presence of genotoxic stress in the mutant strains, DNA staining in damaged cells was performed using propidium iodide (PI). Flow cytometry analyses showed that PI-stained cells represented 17.5, 78.3 and 82.6% of the WT, no. 5 and no. 6 populations, respectively, indicating that the proportion of damaged cells was significantly higher in mutant strains compared with that in the parental strain

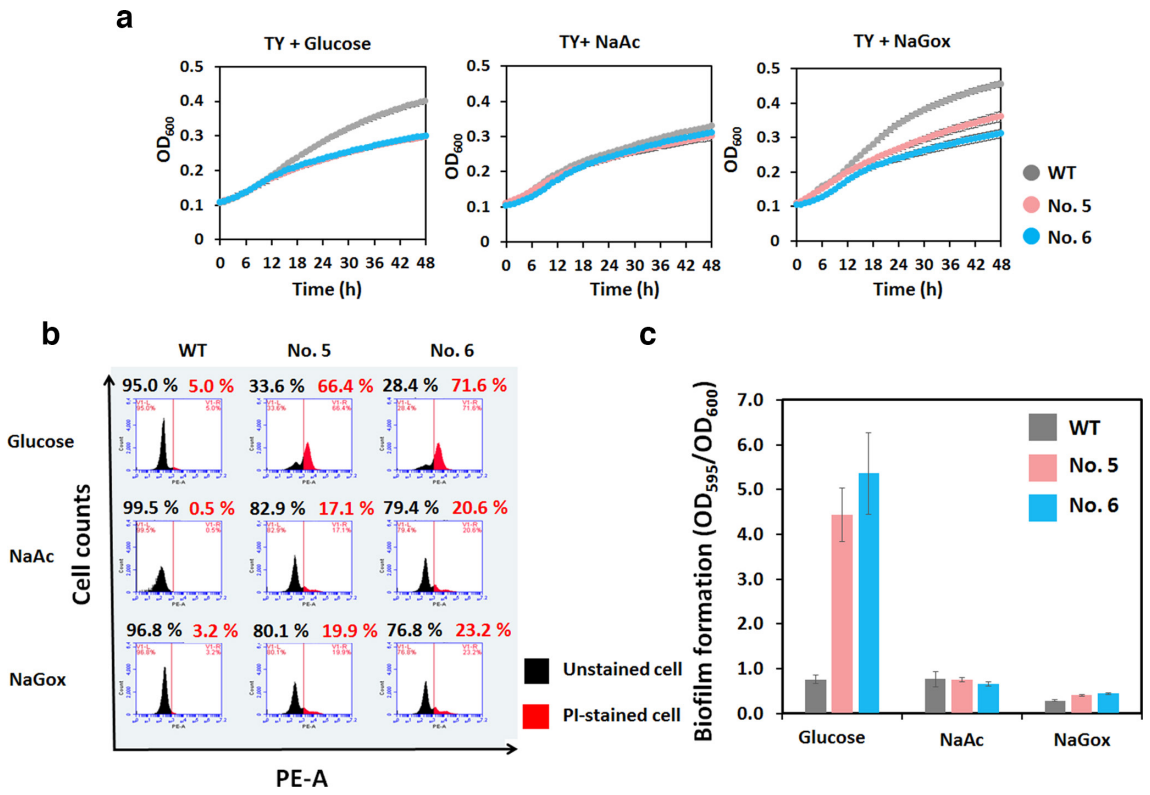

Fig. 5. Mortality and biofilm formation comparison between WT and mutant strains in media with glucose, acetate and glyoxylate supplementation without agitation. (a) Growth of WT and mutant strains in glucose-, acetate- and glyoxylate-supplemented TY medium without agitation. The grey, red and blue lines indicate the growth curves of the WT, no. 5 and no. 6 strains, respectively. All experiments were performed in triplicate, and each of the dots and error bars represents the average and standard deviation of triplicates, respectively. (b) Flow cytometric analysis of PI-stained (red) and non-stained (black) cells in TYG medium after 24 h of cultivation without agitation. The *x*- and *y*-axes represent PE-A (fluorescence intensity) and cell counts, respectively. (c) Quantification of biofilm formation in glucose-, acetate- and glyoxylate-supplemented TY medium at 24 h of culture. NaAc, sodium acetate; NaGox, sodium glyoxylate.

during their growth in TYG medium (Fig. 4b). Additionally, image analyses of dyed DNA and membranes using fluorescence microscopy revealed the presence of compact DNA in the WT strain but not in the mutants; rather, small membrane vesicles were detected in mutant strains nos 5 and 6 within 24 h (Fig. 4c). The protease activity of mutants was 100-fold higher than that of the WT strain (WT, 75.2 μg ml^{-1}; no.5, 13820.4 μg ml^{-1}; and no. 6, 13352.2 μg ml^{-1}), indicating that proteases were highly activated in the mutants (Fig. 4d). These results indicate that stress response-related genes were upregulated in mutant strains and that a high proportion of cells were damaged in mutants, as assessed based on the presence of vesicle production and high protease activity.

Decreased cell mortality and biofilm formation in acetate- and glyoxylate-supplemented TY medium

Activation of the glyoxylate shunt (GS) pathway is among the various survival strategies used by bacteria against stressors such as heat/cold shock, oxidative stress and desiccation [29–33]. Thus, this carbon metabolism pathway was activated in mutant strains to overcome genotoxicity. However, the expression profiles showed that tricarboxylic acid (TCA) cycle-related and electron transfer chain-related genes were consistently expressed in the mutant strain (Table S10). Additionally, GS-related genes, particularly the malate synthase gene (*aceB*), were significantly decreased in mutant no. 6 (*aceA*, 0.8-fold; *aceB*, 0.1-fold). qRT-PCR revealed the downregulation of the *aceA* gene (~0.5-fold) and the upregulation of the *icd* and *sucA* genes in both mutants (Fig. S8a). Interestingly, the gene clusters encoding ATP synthase (*atpABCDEFI*) were upregulated by >1.5-fold in the mutant no. 6 strain (Table S10), and the expression of the *atpD* gene (as confirmed by qRT–PCR) was increased by 2.0±0.4- and 2.8±0.3-fold in no. 5 and no. 6 strains, respectively, compared with that in the WT strain (Fig. S8a). These results led us to hypothesize that respiration via glucose metabolism triggers cell death in the mutants.

To assess this hypothesis, we evaluated mortality and biofilm formation in WT and mutant strains grown in glucose (Glc)-, acetate (NaAc)-, or glyoxylate (NaGox)-supplemented TY medium under static conditions (i.e. without agitation). Regardless of the carbon source and the strain, the OD_{600} value consistently only reached values below 0.5 due to low

oxygen concentration caused by a lack of agitation (Figs 1d and 5a). The growth of WT and mutant strains reached the stationary phase within 48 h in all tested media. However, the WT strain showed growth retardation in the NaAc-supplemented medium, although the growth rates of mutant strains did not vary significantly as a function of carbon substrate (Fig. 5a). In Glc-supplemented media, 5.0, 68.4 and 71.8% of the WT, no. 5 and no. 6 strain populations were damaged cells, respectively. However, a substantially lower number of PI-stained cells was detected in NaAc- and NaGox-supplemented media compared with those in the Glc-supplemented medium (Fig. 5b). Furthermore, a significant reduction in biofilm and ECM component concentration was observed in mutant strains cultured in NaAc- and NaGox-supplemented media and the amounts of biofilm detected in the WT and mutant strains were largely similar (Figs 5c and S8b–d). In conclusion, mutant strains during acetate and glyoxylate metabolism under static conditions exhibited significant reductions in mortality, amount of biofilm formation and ECM components.

DISCUSSION

Deinococcus spp. are well-known UV-resistant bacteria. The survival rate of *Escherichia coli* cells was reduced to <0.1% when exposed to 200 J m^{-2} of UV exposure, whereas two *Deinococcus* species (*Deinococcus* sp. LD4 and LD5) were resistant to a dose above 600 J m^{-2} with an approximately 10% survival rate [34]. Additionally, *D. antarcticus*, *D. xinjiangensis* and *D. radiodurans* exhibited 5, 1.7 and 12% survival rates under 810 J m^{-2} of UV exposure [35, 36]. However, a previous study also demonstrated that *D. metallilatus* populations decreased by 10^{-3} when the cells were irradiated with 60 mJ cm^{-2} (60 J m^{-2}) of UV and were found to be approximately 10^3-fold more sensitive to ionizing radiation than *D. radiodurans* [18]. These results imply that *D. metallilatus* is not as resistant to UV exposure as other *Deinococcus* species.

The quantification of ECM components demonstrated that mutant strains produced higher levels of all ECM factors compared with WT bacteria (Fig. 1c), suggesting that the increased levels of eDNA, protein and polysaccharides led to a robust biofilm production by mutants. Compared with the concentration of proteins and saccharides, eDNA concentration was significantly reduced after 48 h, implying a pronounced eDNA production from cells at the exponential and early stationary phases (24 and 48 h), which then decreased in the middle of the stationary phase (72 h) (Fig. 1c, d). Furthermore, strain- and growth-dependent eDNA production might be related to stressor susceptibility. Experiments with *Campylobacter jejuni* demonstrated that eDNA concentration and biofilm formation increased in response to aerobic and starvation stress, which was closely associated with bacterial cell lysis [37]. Moreover, *Pseudomonas aeruginosa* released eDNA through explosive cell lysis under antibiotic stress (ciprofloxacin) and genotoxic stress (mitomycin C), and these events produced membrane vesicles with shattered membranes [38]. Thus, it is expected that a metabolically active state and genomic instability might provide stresses that induce the enhancement of eDNA concentration and biofilm formation.

Mannose and glucose were the major monosaccharides in the EPS of the WT, no. 5 and no. 6 strains, and their ratios were not significantly different among strains (Table S2). This result indicates that EPS synthesis was more pronounced in mutant strains. The sugar composition of EPS for *Deinococcus* species has only been studied in *D. radiodurans*, and was found to mainly contain xylose, galactose and fucose [39]. However, *D. geothermalis*, a species closely related to *D. metallilatus,* possesses a greater abundance of genes related to sugar metabolism enzymes (e.g. for xylose utilization) than *D. radiodurans* [18, 19]. Therefore, the constituents of EPS would be quite different between *D. metallilatus* and *D. radiodurans*.

Genome sequencing showed that *D. metallilatus* carries three independent replicons, including the main chromosome (contig 3), a secondary chromosome (contig 1) and a megaplasmid (contig 2) (Fig. S2). Although the existence of a secondary chromosome among *Deinococcus* species has only been reported in *D. radiotolerans* (Table S11) [40], it is believed that contig 1 in *D. metallilatus* is a secondary chromosome due to (1) its large size, which is generally undetected in mega plasmids (876461 bp), and (2) the presence of an *rrn* operon (Table S3). However, interestingly, the presence of DnaA (TTCTCCCACAT) and RepA (AGACAGCAA) boxes, an iteron (repeated sequences) and an AT-rich region between the *parA* and *repA* genes is characteristic of the origin of replication in plasmids (Fig. S3c), indicating that the secondary chromosome of *D. metallilatus* exhibits the characteristics of both a chromosome and a plasmid.

Comparison of the genomes of the parental and mutant strains showed the presence of a significant deletion in the genomes of strain nos 5 (248417 bp) and 6 (320987 bp), which occurred mainly in the secondary chromosome (Fig. S4). However, the overlapping sequences in the upstream and downstream deleted regions indicated the possibility of homologous recombination via direct repeated sequences in this region (Fig. S5). Moreover, the deletion sites in mutant genomes were located in CpG island clusters on the secondary chromosome, indicating that CpG islands in the bacterial genome are vulnerable to UV irradiation (Fig. 2a), which is consistent with previous reports [26, 27]. Moreover, the BLAST Atlas genome mapping results clearly indicated the presence of DNA fragments in the secondary chromosome of strain nos 5 and 6, which is suggestive of cellular stress (Fig. 2b).

Transcriptome analyses revealed few expressed reads in the common deletion site of mutant genomes (336652–575926 bp in the secondary chromosome), which provides convincing evidence of genome deletion (Table S5). Most of the deleted genes that were related to gluconate and aminosugar metabolism could be complemented by homologous genes; however, homologues of *eda* genes could not be found, and the loss of two *eda* genes was observed (Table S6, Fig. S7a). Growth retardation or cell death was previously reported in an *eda*

knockout strain [41, 42], suggesting that the low growth rate observed for the *D. metallilatus* mutants might result from impaired glucose metabolism (i.e. caused by the loss of *eda* genes). The genes that participate in the synthesis of GDP-glucose and UDP-mannose exhibited relatively constitutive expression, despite a large genomic deletion (Table S7, Fig. 3). Conversely, the EPS synthesis cluster, rather than LPS synthesis, was upregulated in the mutants (Table S8). Previous ECM component quantification data indicated that mutants produced higher concentrations of sugars than the WT (Fig. 1c); thus, intensive EPS synthesis occurred, and the synthesis of EPS precursors was maintained despite the presence of large genomic deletions.

EPS might be produced in a Wzx/Wzy-dependent manner, as shown in Fig. S7b. EPS precursors (mainly GDP-mannose and UDP-glucose or galactose) would be generated by ManC and GalE, which were located on the main chromosome at both ends of the EPS synthesis cluster (Fig. S7b). Moreover, several glycosyltransferases (GlfT1, EpsF, RfaB and GlgA) attach mannose and glucose to glucose, which is incorporated in the lipid phase by undecaprenyl-phosphate glucose phosphotransferase (WcaJ) (Fig. S7b). Despite the presence of *eps* genes (*epsC* and *epsF*), the operon structure was different from the *eps* operon of *Lactobacillus* and other EPS synthesis operons (e.g. xanthan and colanic acid synthesis operons) [43, 44]. Thus, the mechanisms of EPS assembly remain ambiguous. Furthermore, the mechanisms of EPS synthesis induction in the mutants was unclear; however, the RDR global regulator DdrO was located 4.7 kbp upstream of *manC*, and a motif with a sequence that is similar to that of RDR (i.e. a DdrO-binding site) was present in the promoter of the *manC* gene (Fig. S7c). The *ddrO* gene is known to be induced by DNA damage under UV stress in *D. radiodurans* [45]; thus, regulation of the EPS synthesis operon by DdrO is a possible mechanism of EPS induction in mutant strains.

Genes related to genotoxic stress response, histone-like protein synthesis, chaperones and CRISPR/Cas were highly induced in the mutant strain (no. 6) (Table S9 and Fig. 4a). During DNA repair, the amount of eDNA increased in *D. radiodurans* under UV stress because of the export of DNA and the fact that DNA fragments must be enclosed in vesicles to leave the cells [46, 47]. The quantification of dead cells and microscopic analysis indicated that the fragmented DNA in the mutant strains was actively extruded from the cells at this time (Fig. 4c). Additionally, the high intracellular protease activity detected in mutant strains at 24 h was presumably caused by the misreading of proteins encoded by several damaged DNA fragments (Fig. 4d). It is worth noting that the concentration of eDNA in the ECM of mutants was highest at 24 h (Fig. 1c). Thus, eDNA from damaged or dead cells appeared to contribute to biofilm formation, which is consistent with previous studies [48]. For instance, sublethal tobramycin treatment induces biofilm formation in *P. aeruginosa* due to the presence of eDNA from dead cells. Furthermore, this enhancement of biofilm production by eDNA stemming from cell death occurs not only in laboratory conditions but also in microbial communities in the environment [47]. Glucose toxicity was observed in the mutants (Fig. 4b). Moreover, aeration might be harmful to mutants due to oxidative stress. Thus, we supplemented the culture media with NaAc and NaGox, which induce the GS rather than the TCA cycle, and tested WT and mutant strains under static conditions. Although their growth rates did not vary significantly as a function of carbon source (glucose, acetate, or glyoxylate), cell death, biofilm production and ECM component concentrations were reduced in the mutants (Figs 5 and S8b–d). This result indicates that glucose-induced cell death leads to the enhancement of biofilm production. Previous data suggested that the ED pathway adversely affected biofilm formation in *Vibrio cholerae* strain N16961, which was demonstrated by enhanced biofilm formation compared to the WT strain upon inactivation of the ED pathway ($\Delta edd N_{16961}$ strain) [49]. Furthermore, an ED-positive strain was more defensive to oxidative stress than an ED-negative strain in *Pseudomonas putida* KT 2440 and *Campylobacter* spp. due to the generation of redox currency (NADPH) [50, 51]. Therefore, the enhanced biofilm formation in mutant nos 5 and 6 might be attributable to the activity of stress-inducing aerobic glucose metabolism genes

In this study, a strong biofilm-overproducing strain was generated via UV mutagenesis; however, a trade-off between growth and biofilm formation was detected in the mutant strains. The growth retardation of mutant strains was attributed to a very large genetic deletion and DNA fragmentation within the CpG islands in the secondary chromosomes of mutants. Based on transcriptome analyses and various experimental data, we concluded that the observed large genomic deletions resulted in genotoxicity and metabolic toxicity to the mutant cells. Additionally, aerobic glucose metabolism via oxidative respiration caused severe stress to mutant strains, resulting in cell death. In turn, damaged cells contributed large amounts of eDNA to the ECM, thus promoting biofilm formation.

Funding information
This work was supported by the Hyundai motor company and a National Research Foundation of Korea (NRF) grant awarded by the Korean government (MSIP) (no. NRF-2019R1A2C1088452).

Author contributions
C. P., B. S., W. K., H. C., S. P. and W. P. designed the study. C. P., B. S. and W. K. performed all experiments and analyses. C. P. and W. P. wrote the first draft of the manuscript. H. C., S. P. and W. P. provided substantial discussion and modifications. All authors contributed to the final version of the manuscript and approved it.

Conflicts of interest
The authors declare that there are no conflicts of interest.

References
1. Slade D, Radman M. Oxidative stress resistance in *Deinococcus radiodurans*. *Microbiol Mol Biol Rev* 2011;75:133–191.
2. Anderson AW, Nordon HC, Cain RF, Parrish G, Duggan D. Studies on a radio-resistant *Micrococcus*. Isolation, morphology, cultural characteristics, and resistance to γ-radiation. *Food Technol* 1956;10:575–578.

3. Ujaoney AK, Padwal MK, Basu B. Proteome dynamics during post-desiccation recovery reveal convergence of desiccation and gamma radiation stress response pathways in *Deinococcus radiodurans*. *Biochim Biophys Acta Proteins Proteom* 2017;1865:1215–1226.
4. Udupa KS, O'Cain PA, Mattimore V, Battista JR. Novel ionizing radiation-sensitive mutants of *Deinococcus radiodurans*. *J Bacteriol* 1994;176:7439–7446.
5. Zhang YQ, Sun CH, Li WJ, Yu LY, Zhou JQ *et al*. *Deinococcus yunweiensis* sp. nov., a gamma- and UV-radiation-resistant bacterium from China. *Int J Syst Evol Microbiol* 2007;57:370–375.
6. Donlan RM. Biofilm formation: a clinically relevant microbiological process. *Clin Infect Dis* 2001;33:1387–1392.
7. López D, Vlamakis H, Kolter R. Biofilms. *Cold Spring Harb Perspect Biol* 2010;2:a000398.
8. Dragoš A, Kovács Ákos T. The peculiar functions of the bacterial extracellular matrix. *Trends Microbiol* 2017;25:257–266.
9. Panitz C, Frösler J, Wingender J, Flemming HC, Rettberg P. Tolerances of *Deinococcus geothermalis* biofilms and planktonic cells exposed to space and simulated martian conditions in low earth orbit for almost two years. *Astrobiology* 2019;19:979–994.
10. Frösler J, Panitz C, Wingender J, Flemming HC, Rettberg P. Survival of *Deinococcus geothermalis* in biofilms under desiccation and simulated space and martian conditions. *Astrobiology* 2017;17:431–447.
11. Peltola M, Neu TR, Raulio M, Kolari M, Salkinoja-Salonen MS. Architecture of *Deinococcus geothermalis* biofilms on glass and steel: a lectin study. *Environ Microbiol* 2008;10:1752–1759.
12. Manobala T, Shukla SK, Rao TS, Kumar MD. A new uranium bioremediation approach using radio-tolerant *Deinococcus radiodurans* biofilm. *J Biosci* 2019;44:122.
13. Krisko A, Radman M. Biology of extreme radiation resistance: the way of *Deinococcus radiodurans*. *Cold Spring Harb Perspect Biol* 2013;5:pii:a012765.
14. Theodorakopoulos N, Bachar D, Christen R, Alain K, Chapon V. Exploration of *Deinococcus-Thermus* molecular diversity by novel group-specific PCR primers. *Microbiologyopen* 2013;2:862–872.
15. Park C, Jung HS, Park S, Jeon CO, Park W. Dominance of gas-eating, biofilm-forming *Methylobacterium* species in the evaporator cores of automobile air-conditioning Systems. *mSphere* 2020;5:e00761–19.
16. Kim DU, Lee H, Lee S, Park S, Yoon JH *et al*. *Deinococcus aluminii* sp. nov., isolated from an automobile air conditioning system. *Int J Syst Evol Microbiol* 2018;68:776–781.
17. Kim DU, Lee H, Lee S, Park S, Yoon JH *et al*. *Deinococcus multiflagellatus* sp. nov., isolated from a car air-conditioning system. *Antonie van Leeuwenhoek* 2018;111:619–627.
18. Kim DU, Lee H, Lee JH, Ahn JH, Lim S *et al*. *Deinococcus metallilatus* sp. nov. and *Deinococcus carri* sp. nov., isolated from a car air-conditioning system. *Int J Syst Evol Microbiol* 2015;65:3175–3182.
19. Makarova KS, Omelchenko MV, Gaidamakova EK, Matrosova VY, Vasilenko A *et al*. *Deinococcus geothermalis*: the pool of extreme radiation resistance genes shrinks. *PLoS One* 2007;2:e955.
20. Brim H, Venkateswaran A, Kostandarithes HM, Fredrickson JK, Daly MJ. Engineering *Deinococcus geothermalis* for bioremediation of high-temperature radioactive waste environments. *Appl Environ Microbiol* 2003;69:4575–4582.
21. Eom HJ, Park W. Inhibitory effect of taurine on biofilm formation during alkane degradation in *Acinetobacter oleivorans* DR1. *Microb Ecol* 2017;74:821–831.
22. Chiba A, Sugimoto S, Sato F, Hori S, Mizunoe Y. A refined technique for extraction of extracellular matrices from bacterial biofilms and its applicability. *Microb Biotechnol* 2015;8:392–403.
23. Kim HJ, Shin B, Lee YS, Park W. Modulation of calcium carbonate precipitation by exopolysaccharide in *Bacillus* sp. JH7. *Appl Microbiol Biotechnol* 2017;101:6551–6561.
24. Park C, Shin B, Jung J, Lee Y, Park W. Metabolic and stress responses of *Acinetobacter oleivorans* DR1 during long-chain alkane degradation. *Microb Biotechnol* 2017;10:1809–1823.
25. Chu EK, Kilic O, Cho H, Groisman A, Levchenko A. Self-induced mechanical stress can trigger biofilm formation in uropathogenic *Escherichia coli*. *Nat Commun* 2018;9:4087.
26. Ikehata H, Ono T. Significance of CpG methylation for solar UV-induced mutagenesis and carcinogenesis in skin. *Photochem Photobiol* 2007;83:196–204.
27. Ikehata H, Ono T. The mechanisms of UV mutagenesis. *J Radiat Res* 2011;52:115–125.
28. Lim S, Jung JH, Blanchard L, de Groot A. Conservation and diversity of radiation and oxidative stress resistance mechanisms in *Deinococcus* species. *FEMS Microbiol Rev* 2019;43:19–52.
29. Aliyu H, De Maayer P, Cowan D. The genome of the Antarctic polyextremophile *Nesterenkonia* sp. AN1 reveals adaptive strategies for survival under multiple stress conditions. *FEMS Microbiol Ecol* 2016;92:fiw032.
30. Ahn S, Jung J, Jang IA, Madsen EL, Park W. Role of glyoxylate shunt in oxidative stress response. *J Biol Chem* 2016;291:11928–11938.
31. Jeon JM, Lee HI, Sadowsky MJ, Sugawara M, Chang WS. Characterization of a functional role of the *Bradyrhizobium japonicum* isocitrate lyase in desiccation tolerance. *Int J Mol Sci* 2015;16:16695–16709.
32. Park C, Park W. Survival and energy producing strategies of alkane degraders under extreme conditions and their biotechnological potential. *Front Microbiol* 2018;9:1081.
33. Watanabe S, Yamaoka N, Takada Y, Fukunaga N. The cold-inducible ICl gene encoding thermolabile isocitrate lyase of a psychrophilic bacterium, *Colwellia maris*. *Microbiology* 2002;148:2579–2589.
34. Mohseni M, Abbaszadeh J, Nasrollahi OA. Radiation resistant of native *Deinococcus* spp. isolated from the Lout desert of Iran "the hottest place on Earth". *Int J Environ Sci. Technol* 2014;11:1939–1946.
35. Dong N, Li HR, Yuan M, Zhang XH, Yu Y. *Deinococcus antarcticus* sp. nov., isolated from soil. *Int J Syst Evol Microbiol* 2015;65:331–335.
36. Peng F, Zhang L, Luo X, Dai J, An H *et al*. *Deinococcus xinjiangensis* sp. nov., isolated from desert soil. *Int J Syst Evol Microbiol* 2009;59:709–713.
37. Feng J, Ma L, Nie J, Konkel ME, Lu X. Environmental stress-induced bacterial lysis and extracellular DNA release contribute to *Campylobacter jejuni* biofilm formation. *Appl Environ Microbiol* 2018;84:e02068–17.
38. Turnbull L, Toyofuku M, Hynen AL, Kurosawa M, Pessi G *et al*. Explosive cell lysis as a mechanism for the biogenesis of bacterial membrane vesicles and biofilms. *Nat Commun* 2016;7:11220.
39. Lin SM, Baek CY, Jung JH, Kim WS, Song HY *et al*. Antioxidant activities of an exopolysaccharide (DeinoPol) produced by the extreme radiation-resistant bacterium *Deinococcus radiodurans*. *Sci Rep* 2020;10:55.
40. Charaka VK, Misra HS. Functional characterization of the role of the chromosome I partitioning system in genome segregation in *Deinococcus radiodurans*. *J Bacteriol* 2012;194:5739–5748.
41. Kim J, Yeom J, Jeon CO, Park W. Intracellular 2-keto-3-deoxy-6-phosphogluconate is the signal for carbon catabolite repression of phenylacetic acid metabolism in *Pseudomonas putida* KT2440. *Microbiology* 2009;155:2420–2428.
42. Chen X, Schreiber K, Appel J, Makowka A, Fähnrich B *et al*. The Entner-Doudoroff pathway is an overlooked glycolytic route in cyanobacteria and plants. *Proc Natl Acad Sci U S A* 2016;113:5441–5446.
43. Zeidan AA, Poulsen VK, Janzen T, Buldo P, Derkx PMF *et al*. Polysaccharide production by lactic acid bacteria: from genes to industrial applications. *FEMS Microbiol Rev* 2017;41:S168–S200.
44. Schmid J, Sieber V, Rehm B. Bacterial exopolysaccharides: biosynthesis pathways and engineering strategies. *Front Microbiol* 2015;6:496.
45. Devigne A, Ithurbide S, Bouthier de la Tour C, Passot F, Mathieu M *et al*. DdrO is an essential protein that regulates the radiation desiccation response and the apoptotic-like cell death in the radioresistant *Deinococcus radiodurans* bacterium. *Mol Microbiol* 2015;96:1069–1084.

46. Boling ME, Setlow JK. The resistance of *Micrococcus radiodurans* to ultraviolet radiation: III. *Biochim Biophys Acta* 1966;123:26–33.
47. Ibáñez de Aldecoa AL, Zafra O, González-Pastor JE. Mechanisms and regulation of extracellular DNA release and its biological roles in microbial communities. *Front Microbiol* 2017;8:1390.
48. Tahrioui A, Duchesne R, Bouffartigues E, Rodrigues S, Maillot O *et al*. Extracellular DNA release, quorum sensing, and PrrF1/F2 small RNAs are key players in *Pseudomonas aeruginosa* tobramycin-enhanced biofilm formation. *NPJ Biofilms Microbiomes* 2019;5:15.
49. Patra T, Koley H, Ramamurthy T, Ghose AC, Nandy RK. The Entner-Doudoroff pathway is obligatory for gluconate utilization and contributes to the pathogenicity of *Vibrio cholerae*. *J Bacteriol* 2012;194:3377–3385.
50. Chavarría M, Nikel PI, Pérez-Pantoja D, de Lorenzo V. The Entner-Doudoroff pathway empowers *Pseudomonas putida* KT2440 with a high tolerance to oxidative stress. *Environ Microbiol* 2013;15:1772–1785.
51. Vegge CS, Jansen van Rensburg MJ, Rasmussen JJ, Maiden MCJ, Johnsen LG *et al*. Glucose metabolism via the Entner-Doudoroff pathway in *Campylobacter*: a rare trait that enhances survival and promotes biofilm formation in some isolates. *Front Microbiol* 2016;7:7.